Journal of Geophysical Research: Oceans

RESEARCH ARTICLE
10.1029/2017JC013516

Surface Ocean Enstrophy, Kinetic Energy Fluxes, and Spectra From Satellite Altimetry

Hemant Khatri[1], Jai Sukhatme[2,3], Abhishek Kumar[4], and Mahendra K. Verma[4]

[1]Department of Mathematics, Imperial College London, London, UK, [2]Centre for Atmospheric & Oceanic Sciences, Indian Institute of Science, Bangalore, India, [3]Divecha Centre for Climate Change, Indian Institute of Science, Bangalore, India, [4]Department of Physics, Indian Institute of Technology, Kanpur, India

Key Points:
- Ocean surface mesoscale dynamics is in accord with quasi-geostrophic turbulence
- Kinetic energy flux is upscale and enstrophy cascades downscale

Correspondence to:
H. Khatri,
h.khatri16@imperial.ac.uk

Citation:
Khatri, H., Sukhatme, J., Kumar, A., & Verma, M. K. (2018). Surface ocean enstrophy, kinetic energy fluxes, and spectra from satellite altimetry. *Journal of Geophysical Research: Oceans*, *123*, 3875–3892. https://doi.org/10.1029/2017JC013516

Received 28 SEP 2017
Accepted 24 APR 2018
Accepted article online 4 MAY 2018
Published online 26 MAY 2018

Abstract Spectra and fluxes of enstrophy and kinetic energy (KE) are estimated in different parts of the midlatitudinal oceans using geostrophic currents derived from altimetry data. The presence of a strong inverse flux of surface KE is confirmed at scales larger than approximately 200 km, whereas a robust enstrophy cascading regime, accompanied by an approximate k^{-3} KE spectrum, is observed from about 200 to 100 km. The character of fluxes and spectra is shown to compare favorably with those from a comprehensive Earth system model. In addition, as gridded altimeter data are affected by smoothening and interpolation, the qualitative robustness of the results is verified by sensitivity experiments using space and time-filtered output from the Earth system model. Given the rotational character of the flow, this large-scale inverse KE and smaller-scale forward enstrophy transfer scenario is consistent with expectations from three-dimensional rapidly rotating and strongly stratified turbulence studies as well as detailed analyses of spectra and fluxes in the upper-level midlatitude troposphere. In further accord with results from the atmosphere, decomposing the currents into stationary and eddy components (demarcated here by variability greater and less than 100 days, respectively), it is seen that, in addition to the eddy-eddy contribution, the stationary-eddy and stationary-stationary fluxes play a significant role in the inverse (forward) flux of KE (enstrophy). Thus, it is quite possible that, from about 200 to 100 km, the altimeter is capturing the rotationally dominated portion of a surface oceanic counterpart of the upper tropospheric Nastrom-Gage spectrum.

1. Introduction

For the past decade, satellite altimetry data have been used to estimate the interscale transfer and spectral distribution of surface kinetic energy, henceforth abbreviated as KE, in the oceans. In midlatitudinal regions (e.g., near the Gulf Stream, Kuroshio, and Agulhas currents) with strong eddy activity, the spectral flux of KE in mesoscales (order of few hundreds of km) is seen to be scale dependent. In particular, it has been noted that surface KE tends to be transferred upscale in scales larger than the local deformation radius and downscale in smaller scales (Arbic et al., 2014; Scott & Wang, 2005; Tulloch et al., 2011). Mesoscale wave number spectra of KE, on the other hand, are somewhat diverse with spectral slopes ranging from $-\frac{5}{3}$ to -3 depending on the region in consideration (Le Traon et al., 2008; Stammer, 1997; Xu & Fu, 2012). Further, along-track raw and gridded altimeter data have been employed for the estimation of spectra, and it is generally seen that gridded data tend to produce steeper spectra in mesoscales due to the inherent spatial and temporal smoothening (Wortham, 2012; Wortham & Wunsch, 2014). Interpreting these results concerning the KE flux and spectra in terms of the dynamics captured by the altimeter and, more fundamentally, the nature of the actual dynamics of the upper ocean has been the subject of numerous recent investigations (see e.g., the discussions in Lapeyre, 2009 and Ferrari and Wunsch, 2010).

As baroclinic modes are intensified near the surface (Smith & Vallis, 2001; Wunsch, 1997), it has been suggested that altimetry data mostly represent the first baroclinic mode in the ocean (Stammer, 1997). Indeed, the energy is expected to be concentrated in the first baroclinic mode due to an inverse transfer among the vertical modes (Fu & Flierl, 1980). Given this, at first sight, the observed inverse transfer of surface KE at large scales was surprising, as the classical quasi-geostrophic (QG) baroclinic turbulence anticipates a forward cascade in the baroclinic mode with energy flowing toward the deformation scale (Hoyer & Sadourny, 1982; Salmon, 1980). However, a careful examination of the energy budget in numerical simulations reveals that, while KE cascades to larger scales, the total energy in the first baroclinic mode does indeed flow downscale

(Scott & Arbic, 2007); a feature that is comforting in the context of the traditional theory. In fact, along with the two-layer QG study of Scott and Arbic (2007), inverse transfer of KE has also been documented in more comprehensive ocean models (Aluie et al., 2017; Arbic et al., 2014; Schlösser & Eden, 2007; Venaille et al., 2011). However, the relatively smaller forward flux of KE at small scales is more delicate, and is possibly a result of the limited resolution of the altimetry data (Arbic et al., 2013).

Noting the significance of surface buoyancy gradients (a fact missed in the aforementioned first baroclinic mode framework), it has been suggested that surface QG (SQG) dynamics (Blumen, 1978; Held et al., 1995; Lapeyre, 2017) is a more appropriate framework for the oceans' surface (Klein et al., 2008; Lapeyre & Klein, 2006; Sasaki & Klein, 2012), and is reflected in the altimeter measurements (Lapeyre, 2009). Though the variance of buoyancy is transferred downscale (Pierrehumbert et al., 1994; Sukhatme & Pierrehumbert, 2002), even in the presence of an ambient buoyancy gradient (Sukhatme & Smith, 2009), surface KE actually flows upscale in SQG dynamics (Capet et al., 2008a; Smith et al., 2002), consistent with the flux calculations using altimetry data. Recognizing the importance of both these approaches, there are ongoing efforts to represent the variability of the ocean surface and interpret the altimetry data in terms of a combination of interior and surface QG modes (Lapeyre, 2009; Scott & Furnival, 2012; Smith & Vanneste, 2013).

Thus, much of the work using altimeter data has focused on the inverse transfer of KE at relatively large scales ($\gtrsim$300 km). Here we shift our focus on slightly smaller scales ($\lesssim$300 km) that are still fairly well resolved in the data set. Specifically, in addition to the KE flux, we also compute the spectral flux of enstrophy that sheds new light on the dynamics in a range of scales that span approximately 200–100 km. We find that the enstrophy flux is strong and directed to small scales over this range, and is accompanied by a KE spectrum that follows an approximate k^{-3} power law. This suggests that the rotational currents as derived from the altimeter are in an enstrophy cascading regime from about 200 to 100 km, and in an inverse KE transfer regime for scales greater than about 200 km. Further, in terms of an eddy and slowly varying or stationary decomposition (defined as shorter and longer than 100 day time scale variability, respectively), we observe that the stationary-stationary and stationary-eddy fluxes play a significant role in the net interscale transfer of KE and enstrophy.

Given that smoothening and interpolation inherent in the altimetry product can affect estimates of spectra and fluxes, we present a systematic analysis of space and time filtering on high-resolution data from a comprehensive Earth system model. Most pertinently, it is seen that, while quantitative estimates are affected, the qualitative nature of the KE and enstrophy fluxes remains unchanged. Indeed, the character of the fluxes and scaling of the KE spectra from altimetry are in accord with the results from the ocean eddy-permitting Earth system model. Finally, we interpret these findings in the context of idealized studies of three-dimensional (3-D), rapidly rotating and stratified turbulence, and also compare them with detailed analyses of midlatitude upper tropospheric spectra and fluxes.

2. Data Analysis and Methodology

2.1. Data Description

Gridded data of sea-surface height (SSH) above geoid from the AVISO project have been used in our analysis. The daily data spanning 21 years (1993–2013) is available at a spatial resolution of $0.25^\circ \times 0.25^\circ$. Horizontal currents from SSH data were computed using geostrophic balance relations and the latitudinal variation of the Coriolis parameter was included in the computations. Note that the data represent the maps of absolute dynamic topography (MADT, delay time gridded data), i.e., sum of sea level anomaly and the mean absolute dynamic topography. Absolute geostrophic velocities were computed using the MADT. In addition to AVISO, we have used 1 year of data from a coupled Earth system model, which was run under present-day greenhouse gas conditions (Small et al., 2014). The ocean component of the model (POP) is a primitive equation model that produces daily data at a spatial resolution of approximately $0.1^\circ \times 0.1^\circ$. In order to compare the results with the AVISO data, we only consider geostrophic velocities, which were computed using the SSH data from POP model. The ageostrophic components of the flow are of course important and will be addressed in future, though some comments about these divergent modes are included in the concluding discussion.

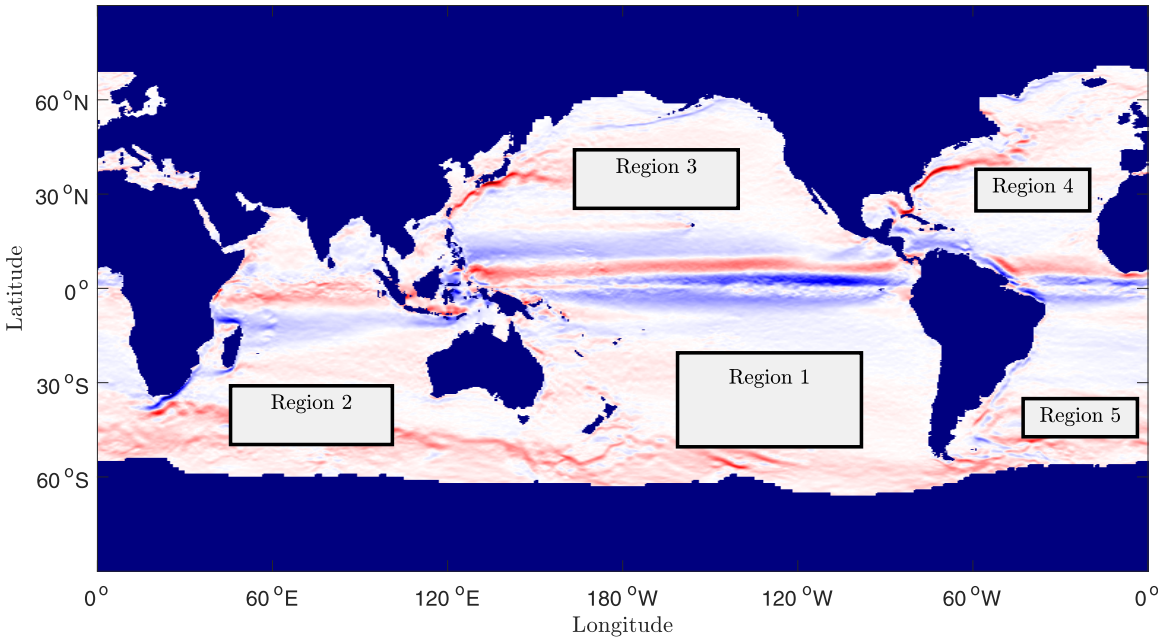

Figure 1. Regions 1–5 chosen for the analysis. Region 1: lat 20° S to 52° S & lon 160° W to 96° W, Region 2: lat 30° S to 46° S & lon 46° E to 110° E, Region 3: lat 25° N to 41° N & lon 155° E to 141° W, Region 4: lat 22° N to 38° N & lon 60° W to 28° W, and Region 5: lat 34° S to 50° S & lon 40° W to 8° W. The 21 year mean of the zonal geostrophic velocity on the ocean surface is shown in color (colorbar range from blue to red is (−1, 1) m/s).

2.2. Geographical Locations

For our analysis, we chose five geographical regions that are located far from the equator so that geostrophic balance is expected to be dominant. As shown in Figure 1, these regions represent relatively uninterrupted stretches in the Southern Indian Ocean, and in the Northern and Southern parts of the Pacific and Atlantic Ocean (exact locations are mentioned in the caption of Figure 1). In essence, we expect that this choice of domain minimizes boundary effects. Region 1 is the largest, and it is about 4,500 km long and 3,500 km wide. Other regions are comparatively smaller.

2.3. Computation of Spectra and Fluxes

In this paper, we compute spectra and fluxes of KE and enstrophy. For this purpose, the velocity field is represented using Fourier modes, i.e.,

$$\mathbf{U}(\mathbf{k}) = \int\int \tilde{\mathbf{U}}(x,y)\exp\left[-\mathrm{i}(k_x x + k_y y)\right]dxdy, \tag{1}$$

where (x, y) are the zonal and meridional directions, $\mathbf{k} = (k_x, k_y)$, and $\tilde{\mathbf{U}} = (u, v)$ contains the zonal and meridional components of the velocity. The two-dimensional (2-D) Fourier transform technique requires the data to have uniform grid spacing in both directions, so a linear interpolation scheme was employed to generate the velocity data on a rectangular grid (the original data were on equidistant latitudes and longitudes). In order to make the velocity field spatially periodic, the data were multiplied with a 2-D bump function ($\exp\left[-\frac{0.01}{1-a^2} - \frac{0.01}{1-b^2} + 0.02\right]$ where $(a, b) \in [-1, 1]$) before performing a Fourier transform, thus, ensuring that the velocity smoothly goes to zero at the boundaries.

We define one-dimensional energy spectrum $E(k)$ as the energy content of a wave number shell $(k - \Delta k < |\mathbf{k}'| \leq k)$:

$$E(k) = \frac{1}{2\Delta k} \sum_{k-\Delta k < |\mathbf{k}'| \leq k} |\mathbf{U}(\mathbf{k}')|^2, \tag{2}$$

where $k = |\mathbf{k}| = \sqrt{k_x^2 + k_y^2}$. In the literature, $E(k)$ is also referred to as the shell spectrum. The temporal evolution of $E(k)$ is given by the following equation (Scott & Wang, 2005):

$$\frac{\partial E(k)}{\partial t} = T(k) + F(k) - D(k), \tag{3}$$

where $F(k)$ is the energy supply rate by an external forcing, $D(k)$ is the energy dissipation at k, and $T(k)$ is the energy supply via nonlinear transfer. In a statistically steady state, $\partial E(k)/\partial t = 0$, and $E(k)$ is approximately constant in time. The energy supply rate due to nonlinearity is balanced by $F(k) - D(k)$.

A useful quantity called KE flux, $\Pi(k)$, measures the energy passing through a wave number of radius k and it is defined as,

$$\Pi(k) = -\int_0^k T(k')dk'. \tag{4}$$

Here

$$T(k) = \frac{1}{\Delta k} \sum_{k-\Delta k < |\mathbf{k}'| \le k} \Re[\mathbf{N}(\mathbf{k}') \cdot \mathbf{U}^*(\mathbf{k}')], \tag{5}$$

$\mathbf{N}(\mathbf{k}')$ is the nonlinear term, and $\Re$ stands for the real part of the argument.

In 2-D flows, another quantity of interest is enstrophy, which is defined as:

$$Z = 1/2 \int \omega^2 d\mathbf{r} = 1/2 \int (\nabla \times \tilde{\mathbf{U}})^2 d\mathbf{r}, \tag{6}$$

where $\omega = \nabla \times \mathbf{u}$ is the vorticity field. The corresponding enstrophy spectrum is defined as:

$$Z(k) = \frac{1}{2\Delta k} \sum_{k-\Delta k < k' \le k} |\omega(\mathbf{k}')|^2. \tag{7}$$

Following a similar procedure as that for $\Pi(k)$, we define an enstrophy flux (denoted by $\zeta(k)$ in the paper), which is a measure of the enstrophy passing through wave number k. Note that there is no transfer of KE and enstrophy from the largest wave number of the system where $\mathbf{U}(\mathbf{k}) \to 0$. Therefore, both KE and enstrophy flux vanish as $k \to \infty$. Further details on spectra and flux computations can be found in Appendix A.

3. Results

We begin by considering the spectra and fluxes associated with daily geostrophic currents. Note that, although AVISO provides daily data, the satellites take 8–10 days to repeat an orbit, so time scales less than a month are not really well resolved by the altimeter data. Figure 2 shows KE and enstrophy spectra of the geostrophic currents derived from the AVISO data in all five regions. As seen, these currents follow an approximate k^{-3} scaling (the best fits range from $k^{-3.2}$ to $k^{-3.6}$) for the KE spectra over a range of 200–100 km in all regions. Consistent with this, the enstrophy spectra follow a power law that is slightly steeper than k^{-1} scaling. At these scales, the KE spectra we obtain for geostrophic currents are more in line with those reported by Stammer (1997), global extratropics, and Arbic et al. (2014), Agulhas region, who used the Ocean Topography Mission (Topex/Poseindon, T/P) data and the gridded altimetry data, respectively. Arbic et al. (2014) also compared the AVISO spectra with a realistic eddying global circulation model and found a good match in the Agulhas region. On the other hand, KE spectra computed using along-track data (from which AVISO gridded product is generated) tend to produce shallower $-\frac{5}{3}$ like scaling, which was observed by Le Traon et al. (2008) (see also, Xu & Fu, 2012, for regional dependency of the exponents).

An important issue here is the effect of smoothening and interpolation in AVISO data on observed spectra (Chelton et al., 2011; Xu & Fu, 2012). Specifically, the scales smaller than 100 km in AVISO data are strongly attenuated because of filtering. In addition, the data in the range 100–200 km are also not completely free from such errors. Keeping this in mind, both along and across-track raw data have been subjected to spectral analysis. Here too, at scales around 200 km, the KE spectra follow power laws but with exponents ranging from -2 (Wortham & Wunsch, 2014) to -3 (Scharffenberg & Stammer, 2011), though the across and along-track exponents can be different (Wortham et al., 2014). In general, spectra computed using the gridded altimetry data tend to be steeper in comparison to spectra estimated using raw along-track data (Wortham, 2012; Wortham & Wunsch, 2014). In this context, Xu and Fu (2012) noted that spectra from the

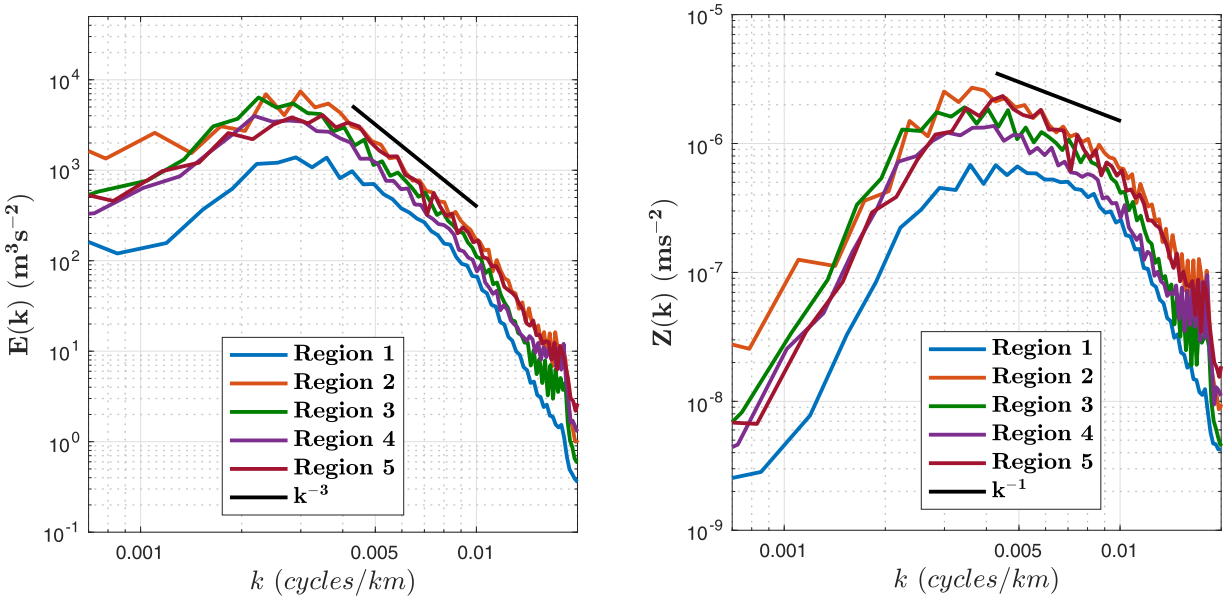

Figure 2. The surface KE and Enstrophy spectra computed using AVISO geostrophic currents (averaged over 21 years of data). For the wave numbers between 0.005 and 0.01 cycles/km (i.e., 200–100 km), the best fits of the spectral exponents for the KE spectra yield −3.31, −3.45, −3.24, −3.60, and −3.65 for the regions 1–5, respectively.

raw along-track data tend to be shallower due to noise in the measurements. In fact, Zhou et al. (2015) used a spatiotemporal filter to remove the high-frequency noise from the raw along-track altimetry data, and in contrast with Le Traon et al. (2008), observed k^{-5} scaling in the SSH spectrum near the Gulf Stream, which corresponds to k^{-3} power law in KE spectrum. However, slopes shallower than k^{-5} were also observed in the SSH spectrum in some regions even after noise removal. Though, it is worth keeping in mind that the ageostrophic part of the SSH data may have contributed to shallowness of the spectra (Zhou et al., 2015).

In ship-track data, exponents ranging between −2 and −3 have been observed in the KE spectrum at scales of approximately 100 km and below in different regions (Callies & Ferrari, 2013; Wang et al., 2010; Wortham et al., 2014). Of course, comparing in situ data with the altimeter is problematic as the former has both rotational and divergent components of the flow. Indeed, a match is only possible if the geostrophic portion is dominant, something one would expect at relatively large scales. For example, a comparison in the Gulf Stream region presented by Callies and Ferrari, (2013) shows altimetry and in situ data to be quite close to each other at scales that range from about 200 to 100 km (both with a −3 scaling). Thus, in all, while caveats regarding the data need to be kept in mind, a −3 scaling of the KE spectrum appears to be a fairly robust feature of AVISO data at length scales from approximately 200 to 100 km.

The KE and enstrophy fluxes for AVISO geostrophic currents are shown in Figure 3. We computed the fluxes using the daily data; the results presented here are averaged over the entire 21 year period. The qualitative structure of the KE flux confirms the findings of Scott and Wang (2005) (see also Arbic et al., 2014; Scott & Arbic, 2007; Tulloch et al., 2011). Specifically, we observe a robust inverse transfer of KE at large scales (i.e., greater than approximately 200 km). Some regions (Regions 1 and 2) show a very weak forward transfer of KE at small scales, while in the others (Regions 3, 4, and 5), the KE flux continues to be negative (though very small in magnitude) even at small scales. In fact, in all the regions considered, the KE flux crosses zero or becomes very small by about 200 km. It should be noted that the forward KE transfer at small scales was more pronounced in Scott and Wang (2005). One of the reasons for this is their use of geostrophic anomalies that tend to produce stronger forward KE flux in comparison to absolute geostrophic velocities. Details regarding this calculation are provided in Appendix B. It is worth pointing out that 2π times the climatological first baroclinic deformation radii in the five regions of Figure 1 also lie between 200 and 250 km (Chelton et al., 1998). Whether this is indicative of a KE injection scale due to baroclinic instability as put forth by Scott and Wang (2005), or more of a coincidence is not particularly clear (we will return to this issue when we examine results from the high-resolution model). Indeed, a mismatch between the deformation scale

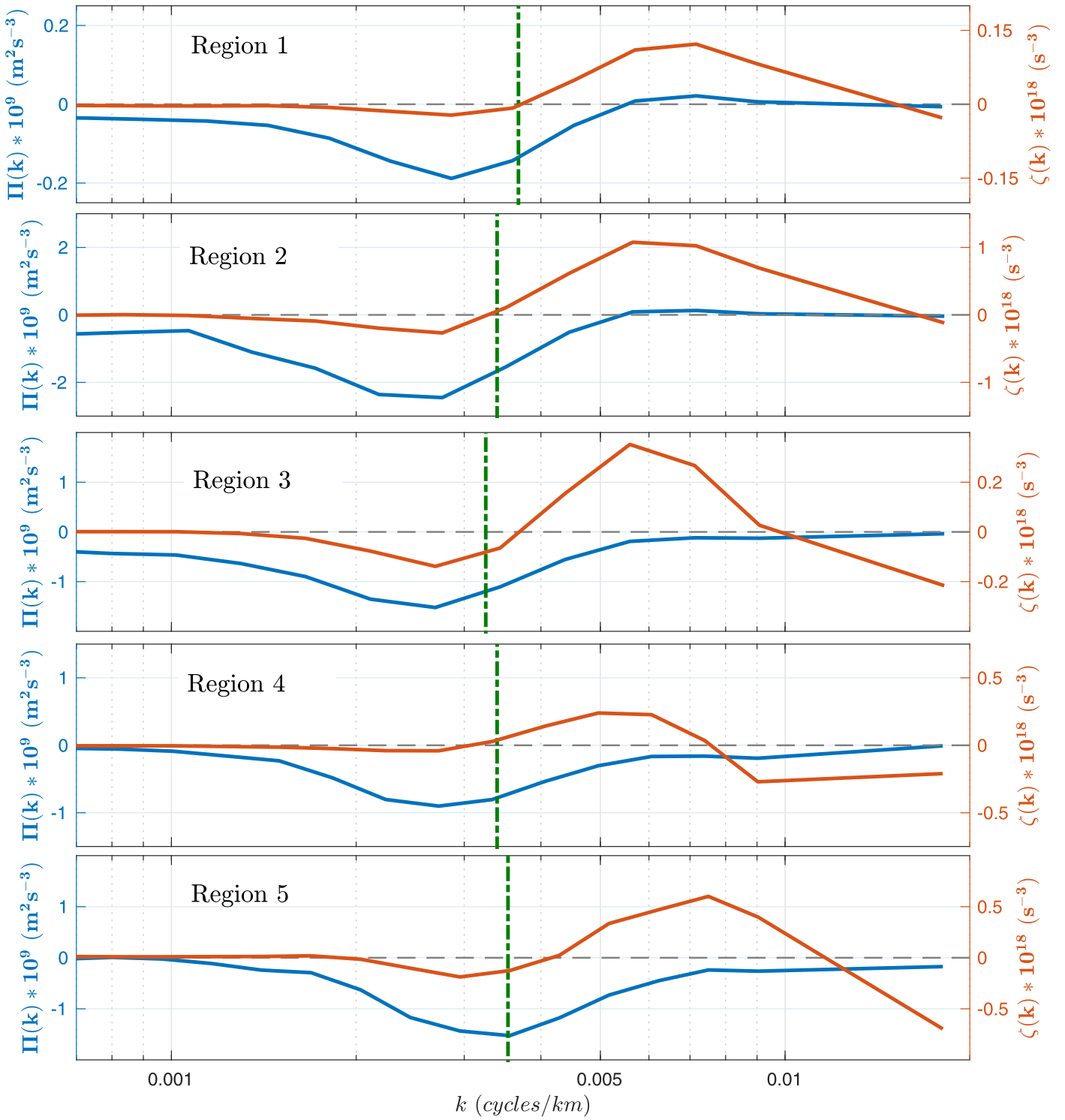

Figure 3. KE ($\Pi(k)$, blue) and enstrophy ($\zeta(k)$, red) fluxes computed using AVISO geostrophic currents (averaged over all 21 years) versus wave number ($k = \sqrt{k_x^2 + k_y^2}$). Vertical dashed lines mark the transition scale ($\sqrt{\langle KE \rangle / \langle Z \rangle}$) in each region.

and zero-crossing scale can be seen in Tulloch et al. (2011) and has also been pointed out by Schlösser and Eden (2007) in a comprehensive ocean model.

Examining the enstrophy fluxes in Figure 3, we observe large forward transfer of enstrophy at scales smaller than approximately 250 km. The enstrophy flux does not show an inertial range in any of the regions; rather

it increases with progressively smaller scales and peaks at approximately 150 km. Note that the enstrophy fluxes do not vanish at the smallest scale, this is due to data interpolation, and is discussed further when comparing with coarsened data from the high-resolution model. Interestingly, we note that, in most of the regions, the scale $\sqrt{\langle KE\rangle/\langle Z\rangle}$ (where $\langle\cdot\rangle$ denotes a domain average; *KE* and *Z* are kinetic energy and enstrophy, respectively) (Danilov & Gurarie, 2000)—shown by the dashed vertical lines in Figure 3—serves as a reasonable marker for the onset of the forward enstrophy flux regime. Thus, from approximately 200 to 100 km, altimetry data suggest the presence of a forward enstrophy transfer regime accompanied by a k^{-3} KE spectrum.

3.1. Comparison With a Comprehensive Earth System Model

We computed spectra and fluxes in the same five oceanic regions using geostrophic currents from the eddy-permitting ocean component (POP) of a comprehensive Earth system model. As mentioned, this model provides us with daily data at a spatial resolution of 0.1°. The main advantage of using this data set is that, unlike AVISO, POP data resolve scales up to 50 km fairly well, and viscous dissipation effects are negligible at scales larger than 100 km (Uchida et al., 2017). The results, shown in Figures 4 and 5, agree very well with the spectra and fluxes from AVISO data. Indeed, the KE and enstrophy spectra from the POP data follow scaling close to k^{-3} and k^{-1}, respectively. In fact, given the higher resolution, the power laws are cleaner than those obtained using the AVISO product. Further, the flux of KE (enstrophy) is predominately upscale (downscale) for large (small) scales in all the regions. However, there are differences between the results from POP and AVISO data, these include: (i) the spectra of KE and enstrophy are slightly steeper in AVISO, (ii) the fluxes are stronger in POP data than in AVISO, especially the enstrophy fluxes, which are almost 5–10 times larger in POP data, (iii) the zero-crossing of the KE flux shifts to smaller scales (approximately 50 km) in all the regions, (iv) the peaks of KE and enstrophy fluxes shift to smaller scales in POP data. Though note that, in accord with the AVISO estimates, the onset of a forward enstrophy flux regime is fairly well predicted by the scale $\sqrt{\langle KE\rangle/\langle Z\rangle}$ (Danilov & Gurarie, 2000). Further, the enstrophy flux gradually increases at larger wave numbers and peaks around 50 km before going to zero at the smallest scale resolved. The same behavior is seen in the AVISO enstrophy fluxes (Figure 3), although the peak is around 150 km. This suggests that estimates of scales where the enstrophy flux peaks and the KE flux crosses zero are probably limited by the resolution of the data. Thus, the observed match between the zero-crossing of rotational KE flux derived from AVISO and the first baroclinic deformation scale (Scott & Wang, 2005), is likely fortuitous.

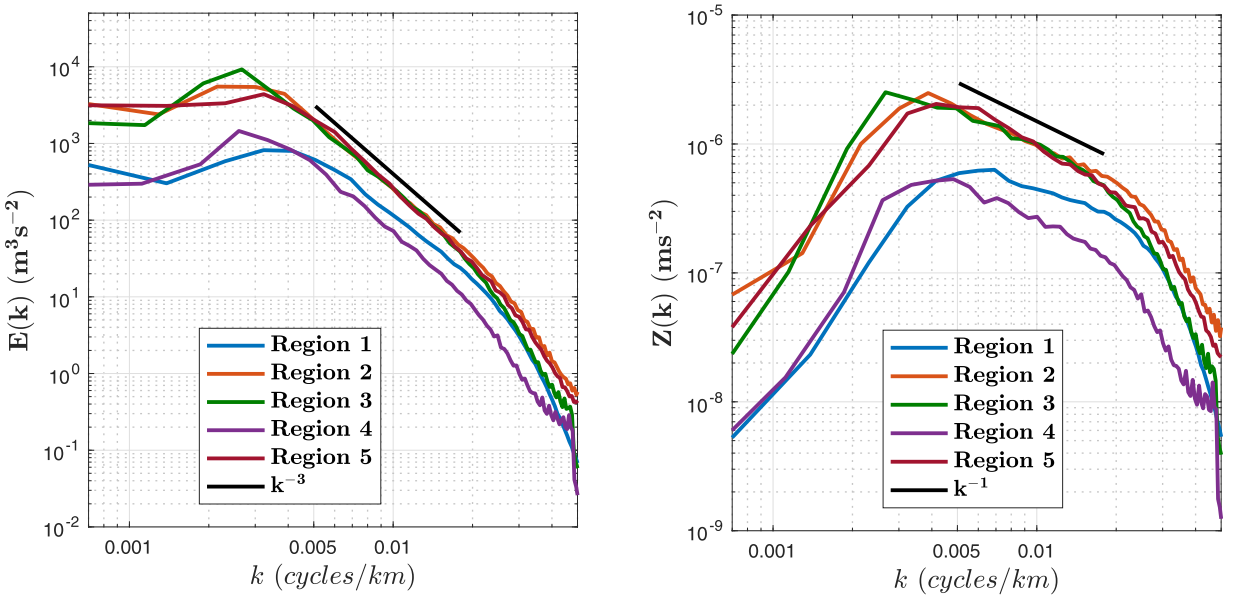

Figure 4. The surface KE and Enstrophy spectra computed using the geostrophic currents from POP model data (averaged over 1 year). For the wave numbers between 0.005 and 0.01 cycles/km (i.e., 200–100 km), the best fits for the spectral exponents for the KE are −2.26, −2.98, −2.91, −2.97, and −2.82 for regions 1–5, respectively.

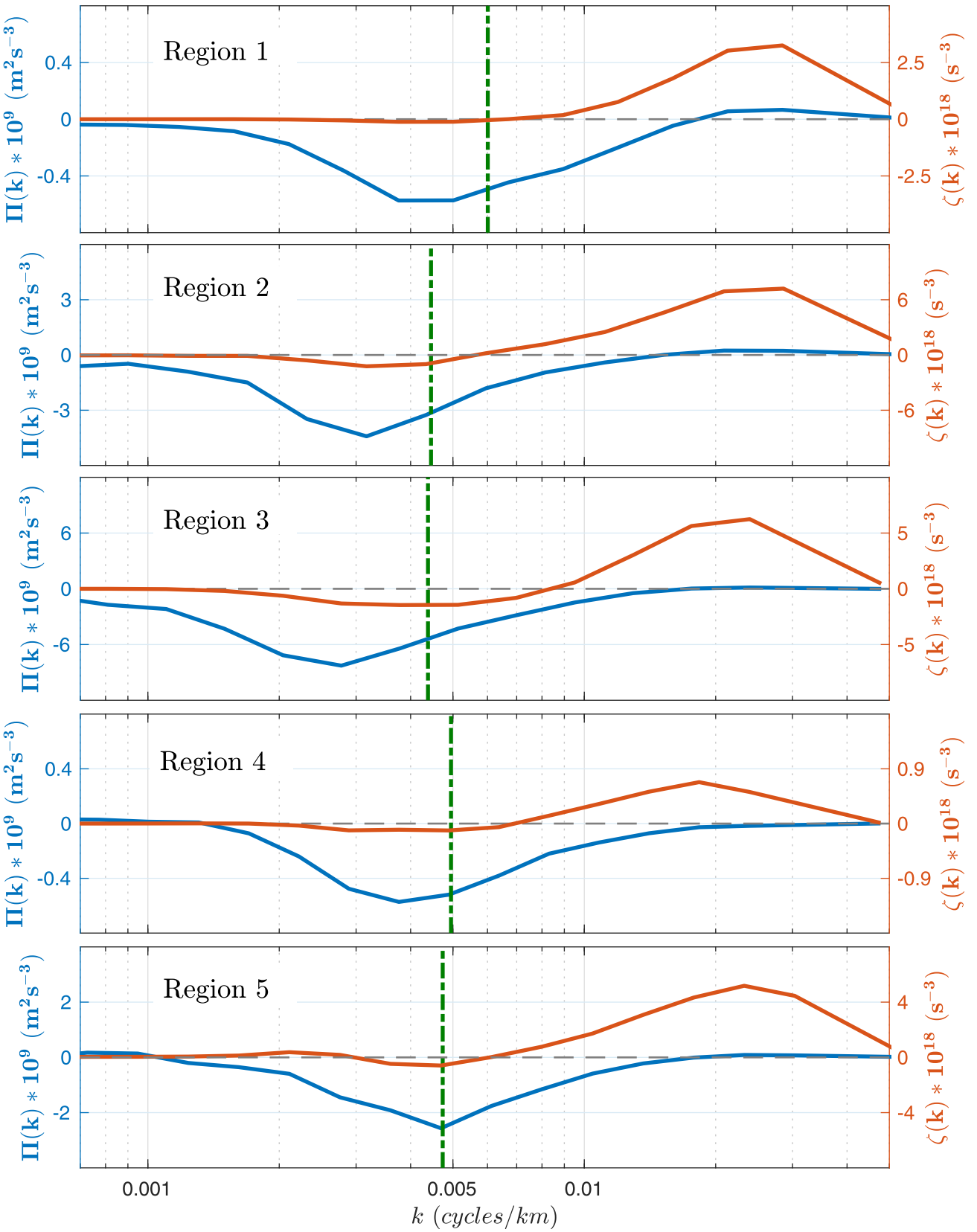

Figure 5. KE ($\Pi(k)$, blue) and enstrophy ($\zeta(k)$, red) fluxes computed using geostrophic currents from POP model data (averaged over 1 year) versus wave number ($k = \sqrt{k_x^2 + k_y^2}$). Vertical dashed lines mark the transition scale ($\sqrt{\langle KE \rangle / \langle Z \rangle}$) in each region.

3.2. Effect of Filtering on Spectra and Fluxes

To probe the issue of the effect of smoothening on the nature of the results in more detail, we proceed with systematic space and/or time filtering tests on the geostrophic currents from POP data. We are also motivated by Arbic et al. (2013), who showed that filtered ocean model output tends to produce an enhanced forward cascade of KE and a reduction in its upscale transfer. We focus on Region 1 for these experiments. In particular, we used geostrophic currents in Region 1 having a grid resolution of roughly 10 km with 400 grid points in both horizontal directions, and computed KE spectra and spectral fluxes using the method described in section 2.3. For filtering in space, the data were generated on coarser 100 × 100 and 50 × 50 grids by averaging over four and eight consecutive grid points, respectively. For smoothening in time, a moving mean was used with 10 and 40 day windows in two separate cases. We believe that these choices, ranging from 100 × 100, 10 day to 50 × 50, 40 day smoothening, would be useful in providing a feel for the impacts of filtering involved in AVISO.

Comparisons between (both) filtered and unfiltered KE fluxes—shown in Figure 6—confirm a decline in the strength of the inverse KE flux due to filtering (in space and time individually, as well as together). In addition, the zero-crossing in the KE flux shifts to larger scales in the filtered data with a presence of forward cascade in all cases. For the enstrophy flux, the strength of forward flux reduces significantly and the peak shifts to larger scales in the filtered data. Interestingly, the zero-crossing of the enstrophy flux is not as sensitive to filtering as for the KE flux curve. Thus, the qualitative behavior of the fluxes remains the same as in the unfiltered data, although the quantitative measures such as the flux strength, zero-crossing and peak scales are sensitive to filtering. Indeed, the enstrophy (KE) flux always shows a robust forward (inverse) transfer at small (large) scales. Note that the fluxes from the spatially filtered data do not vanish at the smallest scale, which is due to the interpolation of the data on the coarser grids. A similar issue was observed in the AVISO enstrophy fluxes (Figure 3). Examining the KE spectrum (shown in Figure 6), we see that it becomes steeper on filtering either in space or time, and the steepening is especially evident in the time-filtered data.

It is instructive to compare the magnitudes of the fluxes from the filtered POP data with AVISO. On moderate smoothening, i.e., 100 × 100 grid and 10 day mean, both KE and enstrophy fluxes are almost twice as large as AVISO estimates in Region 1. On the other hand, with strong smoothening (50 × 50 and 40 day mean), KE and enstrophy fluxes are weaker in strength than the AVISO results. These observations are encouraging as the resolution of the AVISO data lies between these moderate and strong smoothening limits. Using the moderate smoothening stencil in the other oceanic regions under consideration, a comparison between results from AVISO and this moderately smoothened POP data are shown in Figure 7. Fluxes and spectra in Regions 2 and 5 match quite well with AVISO results, but the AVISO fluxes in Regions 1 and 3 are still weaker in strength in comparison to those from the filtered POP data. With regards to Region 4, the

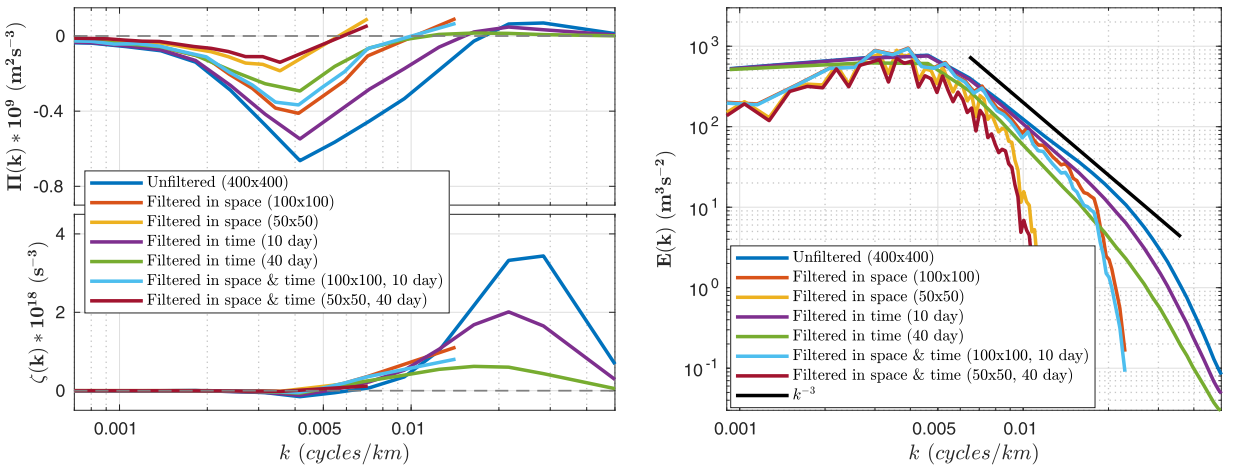

Figure 6. KE and enstrophy fluxes computed using filtered and unfiltered versions of geostrophic currents from POP model data in Region 1 (averaged over 1 year). Filtering in space was performed by averaging over four (eight) grid points in both horizontal directions to generate data on a resolution of 100 × 100 (50 × 50), respectively, whereas the data were filtered in time with 10 and 40 day moving means.

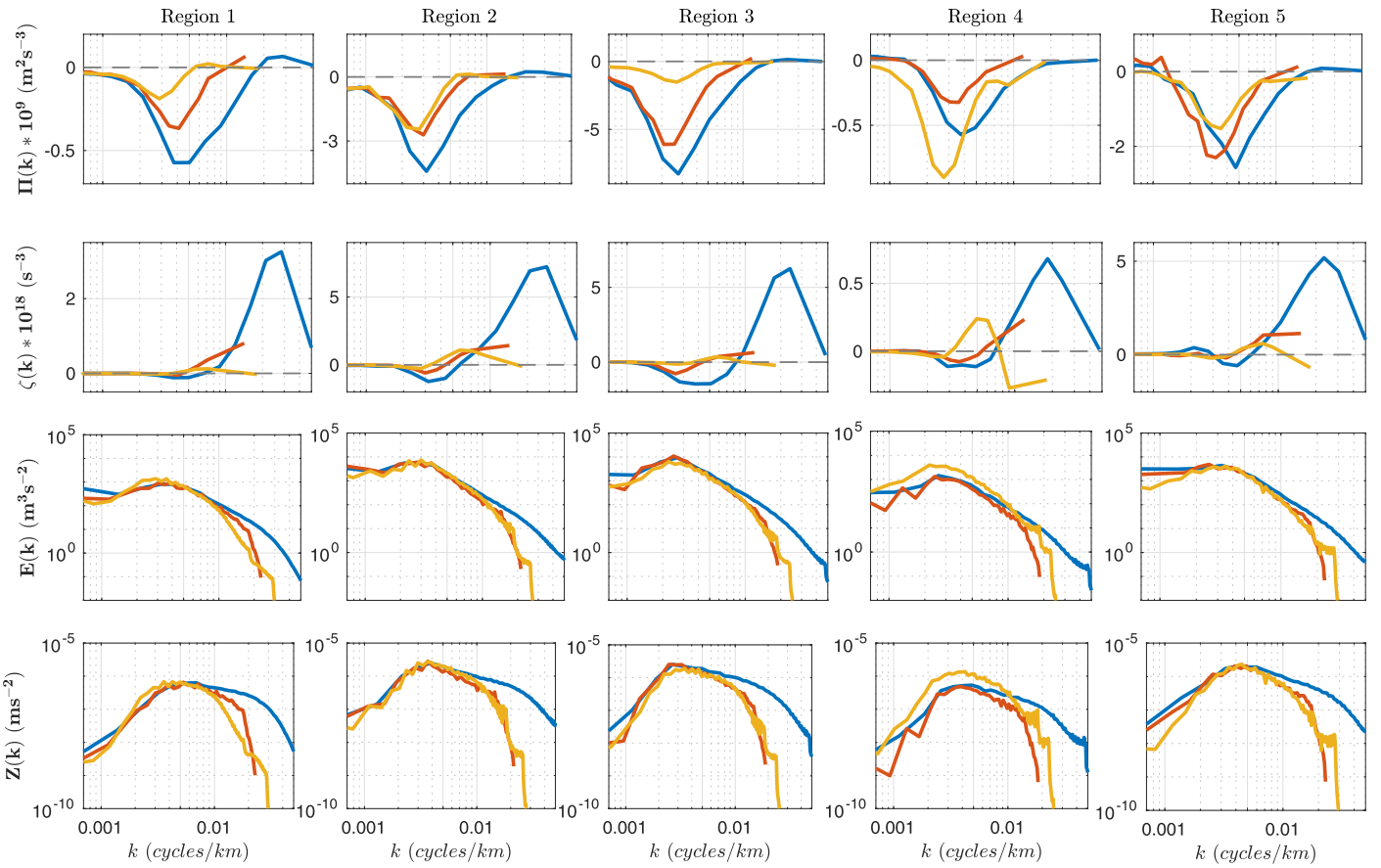

Figure 7. KE and enstrophy fluxes computed using the geostrophic currents from AVISO data (yellow) and POP model data (unfiltered in blue and filtered in red) in all regions.

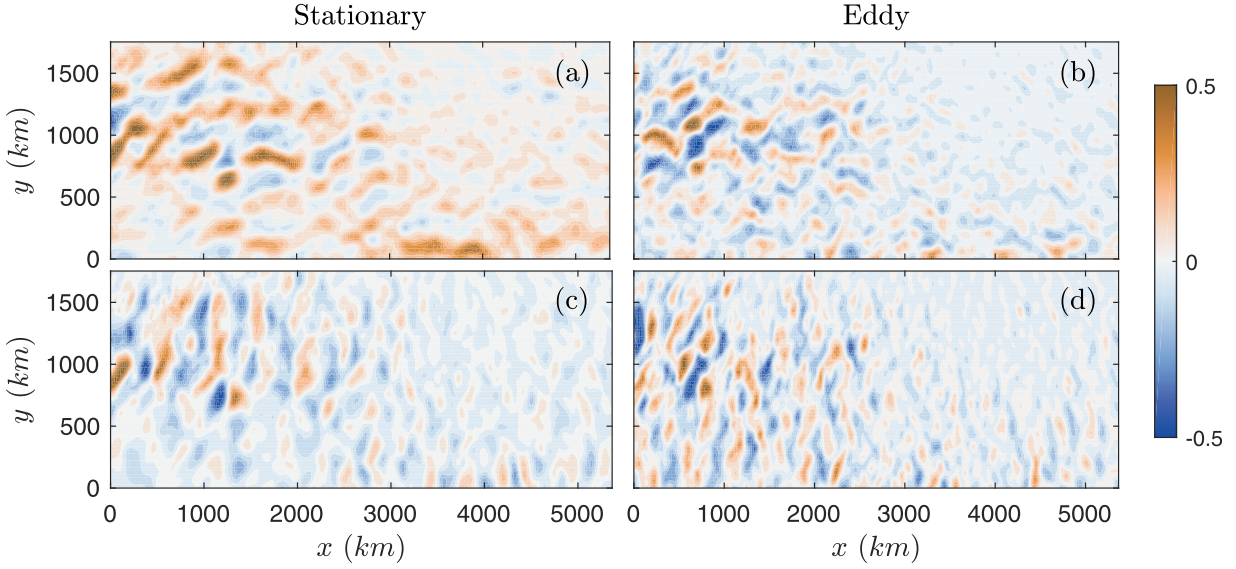

Figure 8. Snapshots of stationary and transient fields (colorbar units are in m/s) from AVISO data—(a), (b) zonal velocity and (c), (d) meridional velocity—in the summer (specifically on 16th June 2005) in Region 3 from AVISO.

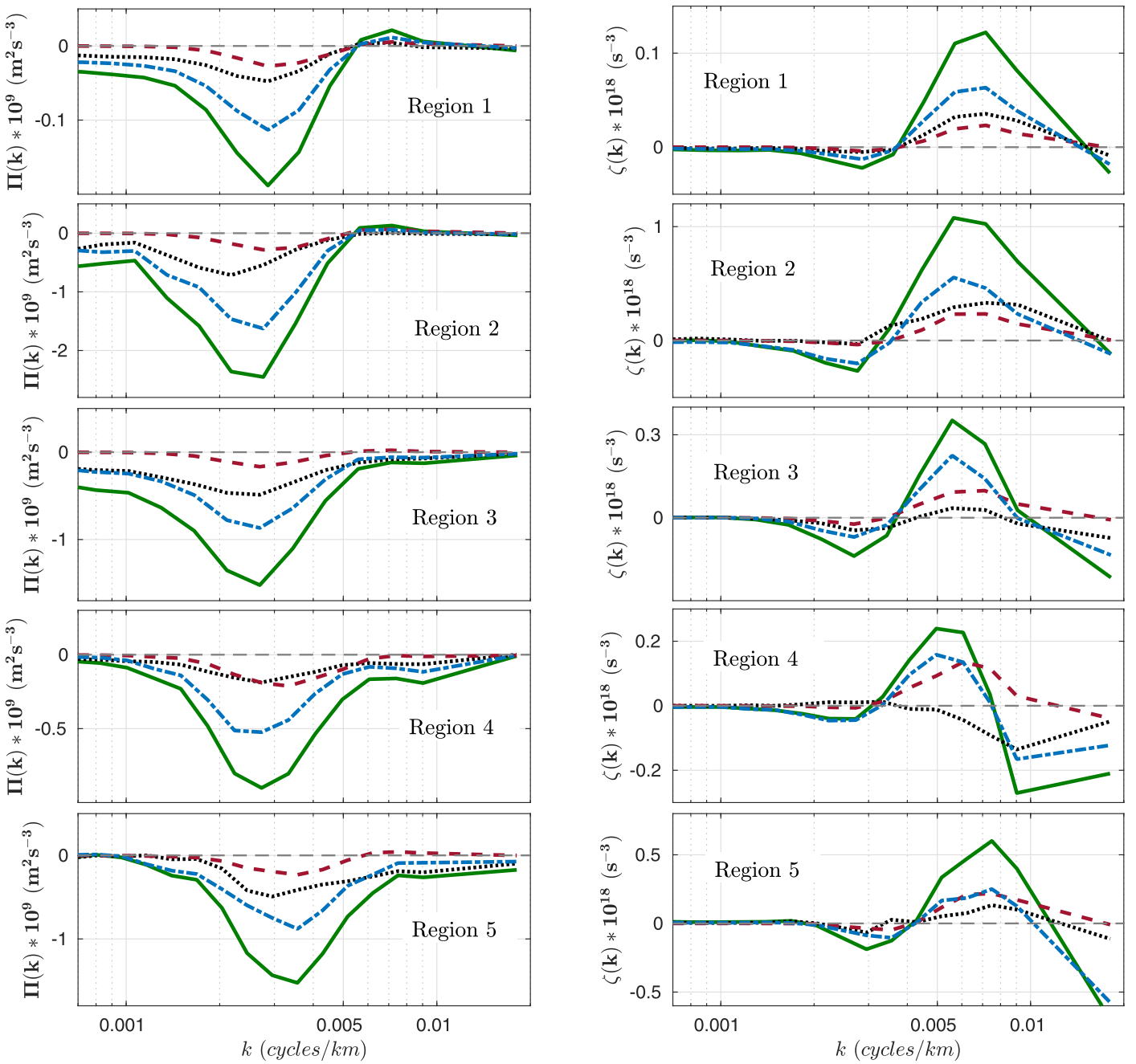

Figure 9. Total (solid green), eddy-eddy (dashed red), stationary-stationary (dotted black), and stationary-eddy (dash-dotted blue) KE and enstrophy fluxes computed using AVISO geostrophic currents (averaged over all 21 years) versus wave number ($k = \sqrt{k_x^2 + k_y^2}$).

KE flux from unfiltered POP data is weaker than that from AVISO, which is surprising as mesocales are resolved much better in POP data than in AVISO. Thus, even though there are differences, this not only reinforces our intuition regarding the effect of smoothening on the fluxes, it also confirms that in all regions, the smoothened POP data (which is close in resolution to AVISO) flux estimates are closer to those from AVISO than from the high-resolution POP data itself.

Taken together, when compared to actual surface ocean dynamics, it is likely that rotational flux estimates (both inverse KE and forward enstrophy) from AVISO data are low, and the weak forward flux of KE at small scales is enhanced and may possibly be spurious. Also, the position of the peak enstrophy flux and

zero-crossing of the KE flux are likely to be over estimates. Nevertheless, the qualitative forms of the KE and enstrophy fluxes and the implied KE and enstrophy transfer regimes are robust.

3.3. Eddy (Transient) and Stationary (Slowly Varying) Fluxes

An important difference between actual geophysical flows (the atmosphere and ocean) and idealized 3-D rotating stratified turbulence is the presence of nontrivial mean flows and a hierarchy of prominent temporal scales. In order to quantify the KE and enstrophy flux contributions from the fast and slowly varying components of the flow, following Shepherd (1987), we filtered the geostrophic currents derived from AVISO. In particular, at every grid point, we consider the daily 21 year long time series and split this into two parts: one that contains variability of less than 100 days (referred to as the "eddy" or "transient" component) and the other with only longer than 100 day time scales (referred to as the "stationary" or "slowly varying"). The

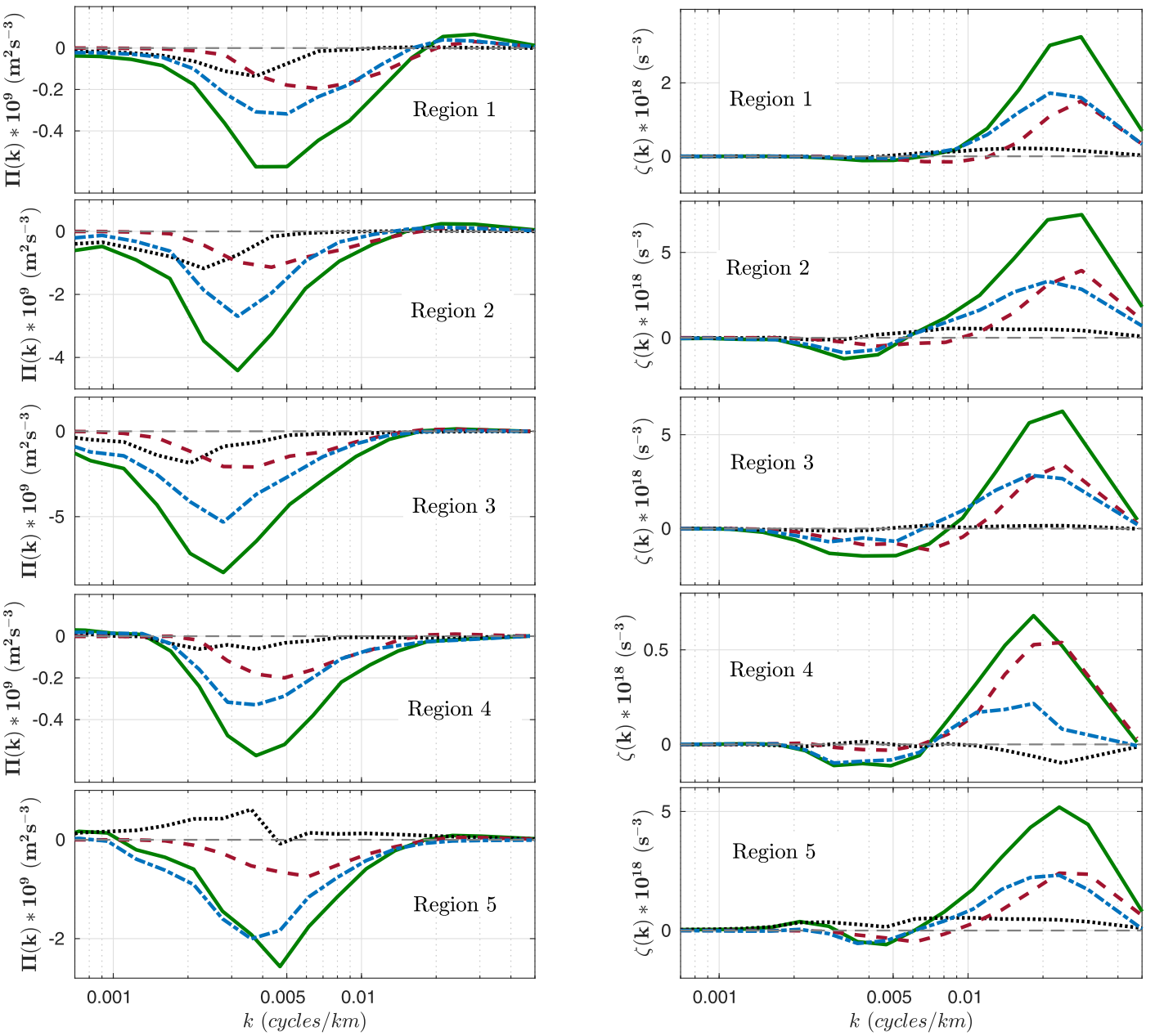

Figure 10. Total (solid green), eddy-eddy (dashed red), stationary-stationary (dotted black) and stationary-eddy (dash-dotted blue) KE and enstrophy fluxes computed using POP model's geostrophic currents (averaged over 1 year) versus wave number ($k = \sqrt{k_x^2 + k_y^2}$).

choice of 100 days is a rough marker to distinguish intraseasonal variability from longer time scales. Our investigation into the role of components is motivated in part by analyses of the troposphere, where it has been shown that both eddy-eddy and eddy-slowly varying interactions contribute significantly to the net interscale KE and enstrophy flux (Burgess et al., 2013; Shepherd, 1987). On a more fundamental level, a handle on these contributions is important as, eddy-eddy interactions come under the purview of isotropic turbulence, while a large contribution from stationary-eddy transfers implies significant wave-mean flow interactions (Shepherd, 1987). To get an idea of the physical character of this decomposition, in Figure 8, we show a snapshot of the zonal and meridional velocities (during summer) in Region 3 from AVISO data. Quite clearly, the slowly varying or stationary flow has a pronounced zonal structure, as compared to the more isotropic eddy component. Similarly, the mean meridional velocity has a larger scale as compared to its eddy component and is oriented in a preferentially meridional direction. It is interesting to note that the meridional (stationary and transient) velocity is always comparable in strength to the zonal flow in all five regions (figures not shown here).

As with the original AVISO data (the total field), we computed the KE and enstrophy fluxes using the transient eddy field and the stationary velocity components. The stationary-eddy fluxes were computed by subtracting the eddy-eddy and stationary-stationary contributions from the total flux. Figure 9 shows these four terms (total: solid green curves, eddy-eddy: dashed red curves, stationary-stationary: dotted black curves and stationary-eddy: dash-dotted blue curves) for both KE and enstrophy in the five regions considered. For the KE, we see that the total flux at large scales (i.e., greater than 200 km) has a strong contribution from the stationary-eddy interactions. In fact, the eddy-eddy term is qualitatively of the correct form, i.e., upscale at scales larger than $\sim$200 km, but quite small in magnitude. The stationary-stationary contribution is always upscale (except for a very small positive bump at small scales in Region 1), and thus, it too enhances the inverse transfer at large scales. For the enstrophy, we see that the eddy-eddy term is reasonably strong, and along with the stationary-eddy flux (in Regions 3, 4, and 5), or both the stationary-stationary and stationary-eddy fluxes (Regions 1 and 2) leads to the strong forward enstrophy cascading regime at small scales (i.e., below approximately 200 km).

We also computed these flux components using the geostrophic currents from POP data (Figure 10). Here too, the eddy-stationary interactions provide strong contributions to the KE and enstrophy fluxes. However, the relative contribution from eddy-eddy interactions is larger in POP data, which is likely due to higher resolution of the model. Indeed, in a similar manner, Shepherd (1987) found stationary-eddy enstrophy fluxes to be important in the atmosphere, but higher resolution data employed in Burgess et al. (2013) suggest that the eddy-eddy term is the dominant contributor to the forward enstrophy flux. Note that the stationary-stationary interactions, which played a role in AVISO, are quite muted in the high-resolution data. Another interesting observation is that peaks of stationary-stationary and eddy-eddy KE fluxes occur at different scales, which was also seen in Shepherd (1987). This is likely due to the scale separation between the slowly varying flow and transient eddy field, even though the scale separation is not as strong as in the atmosphere (see Figure 3 in Shepherd, 1987).

4. Interpretation and Conclusion

Spectral fluxes of KE and enstrophy are estimated using surface geostrophic currents derived from 21 years of AVISO SSH data in different midlatitudinal parts of the world's oceans. Consistent with the previous results (Arbic et al., 2014; Scott & Wang, 2005; Tulloch et al., 2011), we observe that the spectral flux of rotational KE exhibits an inverse transfer at scales larger than about 200 km. Further, at smaller scales, specifically, 200–100 km, we find a strong forward flux of enstrophy accompanied by a KE spectrum that approximately follows a k^{-3} power law. The transition from an inverse KE to a dominant forward enstrophy flux is roughly in agreement with a simple prescription based on the total enstrophy and KE in the domain (Danilov & Gurarie, 2000). The results from AVISO are seen to compare favorably with geostrophic surface ocean data from an eddy-permitting Earth system model. On splitting the data into high (eddy) and low (stationary) frequencies, we observed that both the stationary-stationary and stationary-eddy fluxes play an important role in the inverse (forward) transfer of KE (enstrophy) at scales greater (smaller) than 200 km. Specifically, we find the stationary-eddy term to be important in both AVISO and eddy-permitting model data. In fact, this term dominates over the eddy-eddy contribution in upscale KE transfer. However, the two

terms are of roughly equal strength in the downscale enstrophy transfer. On the other hand, the stationary-stationary contribution is found to be significant only in AVISO data, which is possibly due to the limited resolution of the altimetry product. As discussed by Shepherd (1987) and Burgess et al. (2013), eddy-eddy interactions can be understood within the framework of isotropic 2-D or geostrophic turbulence, but the presence of significant stationary-eddy transfers imply that eddy-mean flow interactions have to be taken into account to understand the turbulence on the ocean surface. We emphasize that spectra and fluxes of KE and enstrophy are affected by the smoothening and interpolation in AVISO data. In particular, as observed from our filtering tests with model data, a lower resolution (in time and/or space) affects the magnitude, zero-crossing, and peak scale of the fluxes. Nevertheless, principal qualitative features of the fluxes, i.e., the inverse (forward) transfer of KE (enstrophy) at large (small) scales, are robust as they remain unchanged under both space and time filtering.

Regarding the small forward flux of rotational KE in AVISO data at scales smaller than approximately 200 km observed in a few regions, the filtering tests suggest that this is likely enhanced, or possibly even an artifact, due to the limited resolution of the altimetry data. This is consistent with regional high-resolution ocean model runs which show a very weak forward rotational KE flux, and that too at very small scales (Capet et al., 2008b). In fact, a similar phenomenon was noted in the atmosphere where a forward KE flux in the rotational modes was observed in the coarse data used by Boer and Shepherd (1983), but it vanishes in the more recent finer scale products analyzed in Augier and Lindborg (2013) and Burgess et al. (2013) (see, Boffetta, 2007, for similar issues in incompressible 2-D turbulence). We now interpret these findings in the context of rapidly rotating, strongly stratified 3-D turbulence as well as spectra and flux analyses from the midlatitude upper troposphere.

Specifically, idealized 3-D rotating Boussinesq simulations suggest that the rotational (or vortical) modes dominate the energy budget at large scales and exhibit a robust inverse transfer of KE to larger scales, and a forward transfer of enstrophy to smaller scales (Bartello, 1995; Kitamura & Matsuda, 2006; Sukhatme & Smith, 2008; Vallgren et al., 2011). These transfers, akin to 2-D and QG turbulence, are accompanied by KE spectra that follow $-\frac{5}{3}$ and -3 power laws in the upscale KE and downscale enstrophy flux dominated regimes (Charney, 1971; Kraichnan, 1967), respectively. Given the rotational nature of the geostrophic currents, our observation of the upscale (downscale) KE (enstrophy) flux at scales greater (smaller) than 200 km is therefore in accordance with the aforementioned expectations. Indeed, the observed scaling in KE spectra is also close to the expected exponent that characterizes the enstrophy flux dominated regime. It should also be noted that the -3 exponent (even in incompressible 2-D turbulence) is fairly delicate. As discussed in the review by Boffetta and Ecke (2012), it is not uncommon to observe power laws for the KE spectrum that range from -3 to -3.5 in the enstrophy cascading regime. An additional caveat that should be kept in mind is that, in this regime, a strict k^{-3} power law is anticipated only in the presence of an inertial range where the forcing and dissipation scales are well separated. However, in the real world, a lack of clear scale separation may lead to spectra that differ from this theoretical expectation.

With regard to the atmosphere, the forward enstrophy transfer regime of QG turbulence has been postulated to explain the -3 portion of midlatitude upper tropospheric KE spectrum (the so-called Nastrom-Gage spectrum, Nastrom & Gage, 1985). Starting from Boer and Shepherd (1983) and Shepherd (1987), in addition to detecting this spectrum in progressively higher resolution general circulation and weather models (see e.g., Hamilton et al., 2008; Koshyk and Hamilton, 2001; Strauss & Ditlevsen, 1999), there have been systematic analyses of the underlying KE and enstrophy fluxes in models as well as reanalysis products (Augier & Lindborg, 2013; Burgess et al., 2013). These studies demonstrate quite clearly that the -3 range of the Nastrom-Gage spectrum (spanning approximately 3,000–4,000 to 500 km in the upper troposphere) corresponds to the dominance of rotational modes with a forward enstrophy cascade. Also, at scales greater than the -3 range (i.e., greater than approximately 4,000 km), the upper troposphere supports an inverse rotational KE flux (Augier & Lindborg, 2013; Burgess et al., 2013). Further, on decomposing the tropospheric flow into eddy and zonal components (which translates to a stationary-eddy decomposition), it is seen that the zonal mean-eddy flux contributes significantly to the inverse KE and forward enstrophy transfer (Burgess et al., 2013; Shepherd, 1987).

Thus, our findings using altimeter data, i.e., employing purely rotational geostrophic currents, at scales larger than approximately 100 km, are in fair accordance with expectations from idealized simulations of rotating stratified flows as well as analyses of upper tropospheric reanalysis and general circulation model

data. The qualitative similarities between the rotational KE fluxes, enstrophy fluxes, KE spectra as well as stationary-eddy contributions to the fluxes of the surface ocean currents and those of the near tropopause atmospheric flow are comforting as both are examples of rapidly rotating and strongly stratified fluids. In fact, in addition to an inverse rotational KE flux at large scales (greater than approximately 200 km), it is quite possible that the altimeter is capturing an enstrophy cascading regime (between 100 and 200 km,

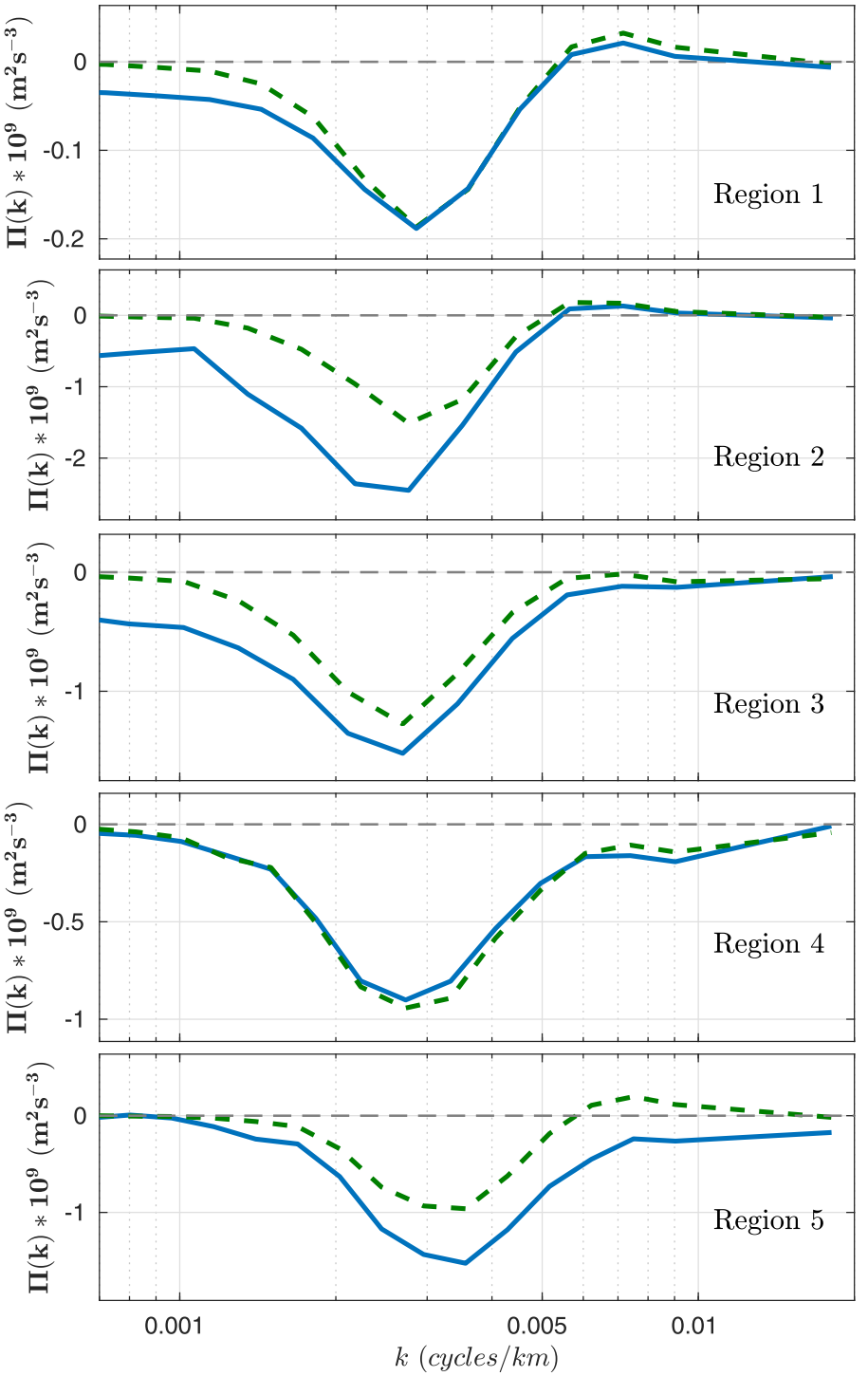

Figure B1. Comparison of KE fluxes (mean over 21 years) computed using full geostrophic velocity field (solid blue) and geostrophic anomaly field (dashed green) from AVISO data in all regions.

accompanied by a relatively steep KE spectrum) that is a surface oceanic counterpart to the -3 range of the atmospheric Nastrom-Gage spectrum.

Quite naturally, it would be very interesting to obtain data at a finer scale, and verify if the KE spectrum of ocean surface currents (rotational and divergent together) exhibits a transition to shallower spectra—like the Nastrom-Gage spectrum—with a change in spectral slope at a length scale smaller than 100 km. Indeed, a flattening of the KE spectrum at scales smaller than 20 km due to an increased contribution of ageostrophic internal waves in the Gulf Stream region has been reported by Callies and Ferrari (2013). Further, recent decompositions of regional high-resolution models (Capet et al., 2008b), and one-dimensional ship-track data have confirmed steep (shallow) scaling of rotational (divergent) modes (Bühler et al., 2014; Qiu et al., 2017; Rocha et al., 2016), with hints at the aforementioned transition in the slope of the KE spectrum (Bühler et al., 2017).

Appendix A: Relations for Spectrum and Flux Computations

Numerical computations of spectra and fluxes were performed at discrete wave numbers. For calculating the spectrum, we used a uniform spacing Δk between two consecutive wave numbers. Specifically, KE and enstrophy spectra in a discretized form were computed using equations (2) and (7).

KE and enstrophy fluxes were estimated using the formalism of Dar et al. (2001), Verma (2004), and Chatterjee et al. (2018), according to which

$$\Pi(k)=\sum_{k'>k}\sum_{p\le k}\delta_{\mathbf{k}',\mathbf{p}+\mathbf{q}}Im([\mathbf{k}'\cdot\mathbf{U}(\mathbf{q})][\mathbf{U}^*(\mathbf{k}')\mathbf{U}(\mathbf{p})]), \tag{A1}$$

$$\zeta(k)=\sum_{k'>k}\sum_{p\le k}\delta_{\mathbf{k}',\mathbf{p}+\mathbf{q}}Im([\mathbf{k}'\cdot\mathbf{U}(\mathbf{q})][\omega^*(\mathbf{k}')\omega(\mathbf{p})]), \tag{A2}$$

where *Im* stands for the imaginary part of the argument, $\mathbf{U}(\mathbf{q})$ and $\omega(\mathbf{q})$ are the Fourier modes of the velocity and vorticity fields, respectively, and $\mathbf{U}^*$ & $\omega*$ are complex conjugates. The expressions (inside the summation operators) in equations (A1) and (A2) represent the energy and enstrophy transfer in a triad ($\mathbf{k}'=\mathbf{p}+\mathbf{q}$), respectively, where $\mathbf{k}'$ mode receives energy (enstrophy) from modes $\mathbf{p}$ and $\mathbf{q}$. These expressions were finally integrated over all possible triads satisfying the condition $k' > k$ and $p \le k$.

Appendix B: Comparison of KE Fluxes Computed Using Full Geostrophic Velocity and Geostrophic Velocity Anomalies

In addition to KE fluxes from full geostrophic velocities, we also computed KE fluxes using the AVISO geostrophic anomalies. These anomalies were obtained by removing the 21 year mean of velocity from the full geostrophic currents. As shown in Figure B1, geostrophic anomalies tend to produce a stronger forward transfer of KE at scales smaller than ~200 km. Also, the KE flux from geostrophic anomalies almost vanishes around 1,000 km scale in all regions. Nevertheless, the KE flux magnitudes in upscale transfer do not change drastically when compared to the estimates from the full geostrophic velocities.

Acknowledgments
The authors declare no conflict of interest. We thank the AVISO project for making the SSH data freely available (http://www.aviso.altimetry.fr/en/home.html). H. K. is supported by President's PhD scholarship and Mathematics of Planet Earth at Imperial College. J. S. would like to acknowledge the support from IITM/MAS/DSG/0001 under the Monsoon Mission funded by the Ministry of Earth Sciences, India. We would like to thank the two anonymous reviewers for their comments and suggestions. In particular, the detailed comments of one of the reviewers helped to significantly improve the manuscript. We also thank Matthew Hecht and Geoff Vallis for providing the POP data (http://www.earthsystemgrid.org/dataset/ucar.cgd.asd.output.html).

References

Aluie, H., Hecht, M., & Vallis, G. K. (2017). Mapping the energy cascade in the North Atlantic Ocean: The coarse-graining approach. *Journal of Physical Oceanography*, *48*, 225–244. https://doi.org/10.1175/JPO-D-17-0100.1

Arbic, B. K., Müller, M., Richman, J. G., Shriver, J. F., Morten, A. J., Scott, R. B., et al. (2014). Geostrophic turbulence in the frequency-wavenumber domain: Eddy-driven low-frequency variability. *Journal of Physical Oceanography*, *44*(8), 2050–2069. https://doi.org/10.1175/JPO-D-13-054.1

Arbic, B. K., Polzin, K. L., Scott, R. B., Richman, J. G., & Shriver, J. F. (2013). On eddy viscosity, energy cascades, and the horizontal resolution of gridded satellite altimeter products. *Journal of Physical Oceanography*, *43*(2), 283–300. https://doi.org/10.1175/JPO-D-11-0240.1

Augier, P., & Lindborg, E. (2013). A new formulation of the spectral energy budget of the atmosphere, with application to two high-resolution general circulation models. *Journal of Atmospheric Sciences*, *70*, 2293–2308. https://doi.org/10.1175/JAS-D-12-0281.1

Bartello, P. (1995). Geostrophic adjustment and inverse cascades in rotating stratified turbulence. *Journal of Atmospheric Sciences*, *52*(24), 4410–4428. https://doi.org/10.1175/1520-0469(1995)052<4410:GAAICI>2.0.CO;2

Blumen, W. (1978). Uniform potential vorticity flow. Part i: Theory of wave interactions and two-dimensional turbulence. *Journal of Atmospheric Sciences*, *35*(5), 774–783. https://doi.org/10.1175/1520-0469(1978)035<0774:UPVFPI >2.0.CO;2

Boer, G. J., & Shepherd, T. G. (1983). Large-scale two-dimensional turbulence in the atmosphere. *Journal of Atmospheric Sciences*, *40*, 164–184. https://doi.org/10.1175/1520-0469(1983)040<0164:LSTDTI>2.0.CO;2

Boffetta, G. (2007). Energy and enstrophy fluxes in the double cascade of two-dimensional turbulence. *Journal of Fluid Mechanics*, *589*, 253–260. https://doi.org/10.1017/S0022112007008014

Boffetta, G., & Ecke, R. E. (2012). Two-dimensional turbulence. *Annual Review of Fluid Mechanics*, *44*, 427–451. https://doi.org/10.1146/annurev-fluid-120710-101240

Bühler, O., Callies, J., & Ferrari, R. (2014). Wave-vortex decomposition of one-dimensional ship-track data. *Journal of Fluid Mechanics*, *756*, 1007–1026. https://doi.org/10.1017/jfm.2014.488

Bühler, O., Kuang, M., & Tabak, E. G. (2017). Anisotropic helmholtz and wave-vortex decomposition of one-dimensional spectra. *Journal of Fluid Mechanics*, *815*, 361–387. https://doi.org/10.1017/jfm.2017.57

Burgess, B., Erler, A., & Shepherd, T. G. (2013). The troposphere-to-stratosphere transition in kinetic energy spectra and nonlinear spectral fluxes as seen in ECMWF analyses. *Journal of Atmospheric Sciences*, *70*, 669–687. https://doi.org/10.1175/JAS-D-12-0129.1

Callies, J., & Ferrari, R. (2013). Interpreting energy and tracer spectra of upper-ocean turbulence in the submesoscale range (1–200 km). *Journal of Physical Oceanography*, *43*(11), 2456–2474. https://doi.org/10.1175/JPO-D-13-063.1

Capet, X., Klein, P., Hua, B. L., Lapeyre, G., & Mcwilliams, J. C. (2008a). Surface kinetic energy transfer in surface quasi-geostrophic flows. *Journal of Fluid Mechanics*, *604*, 165–174. https://doi.org/10.1017/S0022112008001110

Capet, X., McWilliams, J. C., Molemaker, M. J., & Shchepetkin, A. (2008b). Mesoscale to submesoscale transition in the California current system. Part iii: Energy balance and flux. *Journal of Physical Oceanography*, *38*(10), 2256–2269. https://doi.org/10.1175/2008JPO3810.1

Charney, J. (1971). Geostrophic turbulence. *Journal of Atmospheric Sciences*, *28*, 1087–1095. https://doi.org/10.1175/1520-0469(1971)028<1087:GT>2.0.CO;2

Chatterjee, A. G., Verma, M. K., Kumar, A., Samtaney, R., Hadri, B., & Khurram, R. (2018). Scaling of a Fast Fourier Transform and a pseudo-spectral fluid solver up to 196608 cores. *Journal of Parallel and Distributed Computing*, *113*, 77–91. https://doi.org/10.1016/j.jpdc.2017.10.014

Chelton, D. B., Deszoeke, R. A., Schlax, M. G., El Naggar, K., & Siwertz, N. (1998). Geographical variability of the first baroclinic Rossby radius of deformation. *Journal of Physical Oceanography*, *28*(3), 433–460. https://doi.org/10.1175/1520-0485(1998)028<0433:GVOTFB>2.0.CO;2

Chelton, D. B., Schlax, M. G., & Samelson, R. M. (2011). Global observations of nonlinear mesoscale eddies. *Progress in Oceanography*, *91*(2), 167–216. https://doi.org/S0079661111000036

Danilov, S. D., & Gurarie, D. (2000). Quasi-two-dimensional turbulence. *Physics-Uspekhi*, *43*(9), 863–900. https://doi.org/10.1070/PU2000v043n09ABEH000782

Dar, G., Verma, M. K., & Eswaran, V. (2001). Energy transfer in two-dimensional magnetohydrodynamic turbulence: Formalism and numerical results. *Physica D*, *157*(3), 207–225. https://doi.org/10.1016/S0167-2789(01)00307-4

Ferrari, R., & Wunsch, C. (2010). The distribution of eddy kinetic and potential energies in the global ocean. *Tellus, Series A*, *62*(2), 92–108. https://doi.org/10.1111/j.1600-0870.2009.00432.x

Fu, L.-L., & Flierl, G. R. (1980). Nonlinear energy and enstrophy transfers in a realistically stratified ocean. *Dynamics of Atmospheres and Oceans*, *4*(4), 219–246. https://doi.org/10.1016/0377-0265(80)90029-9

Hamilton, K., Takahashi, Y., & Ohfuchi, W. (2008). Mesoscale spectrum of atmospheric motions investigated in a very fine resolution global general circulation model. *Journal of Geophysical Research*, *113*, D18110. https://doi.org/10.1029/2008JD009785

Held, I. M., Pierrehumbert, R. T., Garner, S. T., & Swanson, K. L. (1995). Surface quasi-geostrophic dynamics. *Journal of Fluid Mechanics*, *282*, 1–20. https://doi.org/10.1017/S0022112095000012

Hoyer, J.-M., & Sadourny, R. (1982). Closure modeling of fully developed baroclinic instability. *Journal of Atmospheric Sciences*, *39*(4), 707–721. https://doi.org/10.1175/1520-0469(1982)039<0707:CMOFDB>2.0.CO;2.

Kitamura, Y., & Matsuda, Y. (2006). The $k^{-3}{}_H$ and $k^{-5/3}{}_H$ energy spectra in stratified turbulence. *Geophysical Research Letters*, *33*, L05809. https://doi.org/10.1029/2005GL024996

Klein, P., Hua, B. L., Lapeyre, G., Capet, X., Le Gentil, S., & Sasaki, H. (2008). Upper ocean turbulence from high-resolution 3d simulations. *Journal of Physical Oceanography*, *38*(8), 1748–1763. https://doi.org/10.1175/2007JPO3773.1

Koshyk, J., & Hamilton, K. (2001). The horizontal kinetic energy spectrum and spectral budget simulated by a high-resolution troposphere-stratosphere-mesosphere GCM. *Journal of Atmospheric Sciences*, *58*, 329–348. https://doi.org/10.1175/1520-0469(2001)058<0329:THKESA>2.0.CO;2.

Kraichnan, R. H. (1967). Inertial ranges in two-dimensional turbulence. *Physics of Fluids*, *10*(7), 1417–1423. https://doi.org/10.1063/1.1762301

Lapeyre, G. (2009). What vertical mode does the altimeter reflect? On the decomposition in baroclinic modes and on a surface-trapped mode. *Journal of Physical Oceanography*, *39*(11), 2857–2874. https://doi.org/10.1175/2009JPO3968.1

Lapeyre, G. (2017). Surface quasi-geostrophy. *Fluids*, *2*(1), 7. https://doi.org/10.3390/fluids2010007

Lapeyre, G., & Klein, P. (2006). Dynamics of the upper ocean layers in terms of surface quasigeostrophy theory. *Journal of Physical Oceanography*, *36*(2), 165–176. https://doi.org/10.1175/JPO2840.1

Le Traon, P.-Y., Klein, P., Hua, B. L., & Dibarboure, G. (2008). Do altimeter wavenumber spectra agree with the interior or surface quasigeostrophic theory? *Journal of Physical Oceanography*, *38*(5), 1137–1142. https://doi.org/10.1175/2007JPO3806.1

Nastrom, G., & Gage, K. (1985). A climatology of atmospheric wavenumber spectra of wind and temperature observed by commercial aircraft. *Journal of Atmospheric Sciences*, *42*(9), 950–960. https://doi.org/10.1175/1520-0469(1985)042<0950:ACOAWS>2.0.CO;2

Pierrehumbert, R., Held, I., & Swanson, K. (1994). Spectra of local and nonlocal two-dimensional turbulence. *Chaos, Solitons & Fractals*, *4*(6), 1111–1116. https://doi.org/10.1016/0960-0779(94)90140-6

Qiu, B., Nakano, T., Chen, S., & Klein, P. (2017). Submesoscale transition from geostrophic flows to internal waves in the northwestern pacific upper ocean. *Nature Communications*, *8*, 14055. https://doi.org/10.1038/ncomms14055

Rocha, C. B., Chereskin, T. K., Gille, S. T., & Menemenlis, D. (2016). Mesoscale to submesoscale wavenumber spectra in drake passage. *Journal of Physical Oceanography*, *46*(2), 601–620. https://doi.org/10.1175/JPO-D-15-0087.1

Salmon, R. (1980). Baroclinic instability and geostrophic turbulence. *Geophysical & Astrophysical Fluid Dynamics*, *15*(1), 167–211. https://doi.org/10.1080/03091928008241178

Sasaki, H., & Klein, P. (2012). SSH wavenumber spectra in the north pacific from a high-resolution realistic simulation. *Journal of Physical Oceanography*, *42*(7), 1233–1241. https://doi.org/10.1175/JPO-D-11-0180.1

Scharffenberg, M. G., & Stammer, D. (2011). Statistical parameters of the geostrophic ocean flow field estimated from the Jason-1-TOPEX/Poseidon Tandem Mission. *Journal of Geophysical Research*, *116*, C12011. https://doi.org/10.1029/2011JC007376

Schlösser, F., & Eden, C. (2007). Diagnosing the energy cascade in a model of the north Atlantic. *Geophysical Research Letters*, *34*, L02604. https://doi.org/10.1029/2006GL027813

Scott, R. B., & Arbic, B. K. (2007). Spectral energy fluxes in geostrophic turbulence: Implications for ocean energetics. *Journal of Physical Oceanography*, *37*(3), 673–688. https://doi.org/10.1175/JPO3027.1

Scott, R. B., & Furnival, D. G. (2012). Assessment of traditional and new eigenfunction bases applied to extrapolation of surface geostrophic current time series to below the surface in an idealized primitive equation simulation. *Journal of Physical Oceanography*, *42*(1), 165–178. https://doi.org/10.1175/2011JPO4523.1

Scott, R. B., & Wang, F. (2005). Direct evidence of an oceanic inverse kinetic energy cascade from satellite altimetry. *Journal of Physical Oceanography*, *35*(9), 1650–1666. https://doi.org/10.1175/JPO2771.1

Shepherd, T. G. (1987). A spectral view of nonlinear fluxes and stationary-transient interaction in the atmosphere. *Journal of Atmospheric Sciences*, *44*, 1166–1178. https://doi.org/10.1175/1520-0469(1987)044<1166:ASVONF>2.0.CO;2

Small, R. J., Bacmeister, J., Bailey, D., Baker, A., Bishop, S., Bryan, F., et al. (2014). A new synoptic scale resolving global climate simulation using the community earth system model. *Journal of Advances in Modeling Earth Systems*, *6*(4), 1065–1094. https://doi.org/10.1002/2014MS000363

Smith, K., Boccaletti, G., Henning, C., Marinov, I., Tam, C., Held, I., et al. (2002). Turbulent diffusion in the geostrophic inverse cascade. *Journal of Fluid Mechanics*, *469*, 13–48. https://doi.org/10.1017/S0022112002001763

Smith, K. S., & Vallis, G. K. (2001). The scales and equilibration of midocean eddies: Freely evolving flow. *Journal of Physical Oceanography*, *31*(2), 554–571. https://doi.org/10.1175/1520-0485(2001)031<0554:TSAEOM>2.0.CO;2

Smith, K. S., & Vanneste, J. (2013). A surface-aware projection basis for quasigeostrophic flow. *Journal of Physical Oceanography*, *43*, 548–562. https://doi.org/10.1175/JPO-D-12-0107.1

Stammer, D. (1997). Global characteristics of ocean variability estimated from regional topex/poseidon altimeter measurements. *Journal of Physical Oceanography*, *27*(8), 1743–1769. https://doi.org/10.1175/1520-0485(1997)027<1743:GCOOVE>2.0.CO;2

Strauss, D., & Ditlevsen, P. (1999). Two-dimensional turbulence properties of the ECMWF reanalyses. *Tellus*, *51*, 749–772. https://doi.org/10.1175/JAS-D-12-0129.1

Sukhatme, J., & Pierrehumbert, R. (2002). Surface quasigeostrophic turbulence: The study of an active scalar. *Chaos*, *12*(2), 439–450. https://doi.org/10.1063/1.1480758

Sukhatme, J., & Smith, L. M. (2008). Vortical and wave modes in 3d rotating stratified flows: random large-scale forcing. *Geophysical & Astrophysical Fluid Dynamics*, *102*(5), 437–455. https://doi.org/10.1080/03091920801915318

Sukhatme, J., & Smith, L. M. (2009). Local and nonlocal dispersive turbulence. *Physics of Fluids*, *21*(5), 056603. https://doi.org/10.1063/1.3141499

Tulloch, R., Marshall, J., Hill, C., & Smith, K. S. (2011). Scales, growth rates, and spectral fluxes of baroclinic instability in the ocean. *Journal of Physical Oceanography*, *41*(6), 1057–1076. https://doi.org/10.1175/2011JPO4404.1

Uchida, T., Abernathey, R., & Smith, S. (2017). Seasonality of eddy kinetic energy in an eddy permitting global climate model. *Ocean Modelling*, *118*, 41–58. https://doi.org/10.1016/j.ocemod.2017.08.006

Vallgren, A., Duesebio, E., & Lindborg, E. (2011). Possible explanation of the atmospheric kinetic and potential energy spectra. *Physical Review Letters*, *107*, 268501. https://doi.org/10.1103/PhysRevLett.107.268501

Venaille, A., Vallis, G. K., & Smith, K. S. (2011). Baroclinic turbulence in the ocean: Analysis with primitive equation and quasigeostrophic simulations. *Journal of Physical Oceanography*, *41*(9), 1605–1623. https://doi.org/10.1175/JPO-D-10-05021.1

Verma, M. K. (2004). Statistical theory of magnetohydrodynamic turbulence: Recent results. *Physics Reports*, *401*(5), 229–380. https://doi.org/10.1016/j.physrep.2004.07.007

Wang, D.-P., Flagg, C. N., Donohue, K., & Rossby, H. T. (2010). Wavenumber spectrum in the gulf stream from shipboard ADCP observations and comparison with altimetry measurements. *Journal of Physical Oceanography*, *40*(4), 840–844. https://doi.org/10.1175/2009JPO4330.1

Wortham, C., Callies, J., & Scharffenberg, M. G. (2014). Asymmetries between wavenumber spectra of along-and across-track velocity from tandem mission altimetry. *Journal of Physical Oceanography*, *44*(4), 1151–1160. https://doi.org/10.1175/JPO-D-13-0153.1

Wortham, C., & Wunsch, C. (2014). A multidimensional spectral description of ocean variability. *Journal of Physical Oceanography*, *44*(3), 944–966. https://doi.org/10.1175/JPO-D-13-0113.1

Wortham, C. J. L. IV (2012). *A multi-dimensional spectral description of ocean variability with applications* (PhD thesis). Woods Hole, MA: Massachusetts Institute of Technology.

Wunsch, C. (1997). The vertical partition of oceanic horizontal kinetic energy. *Journal of Physical Oceanography*, *27*(8), 1770–1794. https://doi.org/10.1175/1520-0485(1997)027<1770:TVPOOH>2.0.CO;2

Xu, Y., & Fu, L.-L. (2012). The effects of altimeter instrument noise on the estimation of the wavenumber spectrum of sea surface height. *Journal of Physical Oceanography*, *42*(12), 2229–2233. https://doi.org/10.1175/JPO-D-12-0106.1

Zhou, X.-H., Wang, D.-P., & Chen, D. (2015). Global wavenumber spectrum with corrections for altimeter high-frequency noise. *Journal of Physical Oceanography*, *45*(2), 495–503. https://doi.org/10.1175/JPO-D-14-0144.1